Chitosan as stabilizing agent for negatively charged nanoparticles

Mar Collado-González[a], Mercedes G. Montalbán[b], Jorge Peña-García[c], Horacio Pérez-Sánchez[c], Gloria Víllora[b], F. Guillermo Díaz Baños[a,*]

[a] Department of Physical Chemistry, University of Murcia, Murcia, Spain
[b] Department of Chemical Engineering, University of Murcia, Murcia, Spain
[c] Bioinformatics and High Performance Computing Research Group (BIO-HPC), Computer Engineering Department, Universidad Católica San Antonio de Murcia (UCAM), Murcia, Spain

Keywords:
Chitosan
Gold nanoparticles
Silk fibroin nanoparticles
Aggregation-Stabilizing effect
Dynamic light scattering
Molecular modeling

a b s t r a c t

Chitosan is a biocompatible polysaccharide with positive Z potential which can stabilize negative charged nanoparticles. Silk fibroin nanoparticles and citrate gold nanoparticles, both with negative Z potential, but they form aggregates at physiological ionic strength. In this work, we study the behavior of chitosan in solution when the ionic strength of the medium is increased and how the concentration of chitosan and the proportion of the two components (chitosan and AuNP or SFN) significantly affect the stability and size of the nanocomposites formed. In addition to experimental measurements, molecular modeling were used to gain insight into how chitosan interacts with silk fibroin monomers, and to identify the main energetic interactions involved in the process. The optimum values for obtaining the smallest and most homogeneous stable nanocomposites were obtained and two different ways of organization through which chitosan may exert its stabilizing effect were suggested.

1. Introduction

Nanomedicine, especially as regard the design of drug delivery systems, has seen significant progress in recent decades (Cho, Bégin, & Carreau, 2006; Mottaghitalab, Farokhi, Shokrgozar, Atyabi, & Hosseinkhani, 2015). However, in many cases the problem arises that nanoparticles tend to aggregate upon exposure to biological media (Wang, Xu, Yang, & Shao, 2015; Zakaria et al., 2013). To prevent this, chitosan has been proposed as a stabilizing agent for both metallic (Leiva et al., 2015) and non metallic (Luo, Teng, Li, & Wang, 2015) nanoparticles. This will be the focus of the present study.

Chitosan (CS) is a linear biopolymer with a complex behavior (Domard, 2011). Its biodegradability, biocompatibility and non-toxicity (Delmar & Bianco-Peled, 2015), and its antibacterial activity (Raferty, Tierney, Curtin, Cryan, & O'Brien, 2015) are the reasons why micro and nanoparticles of chitosan are used in several fields and applications (Leiva et al., 2015). Chitosan is a good option for stabilizing nanoparticles due to its polycationic nature (Raferty et al., 2015) and its conformation in solution (Morris, Castile, Smith, Adams, & Harding, 2009). Suspensions of some nanoparticles remain stable because of the electrostatic repulsion between negative charges on their surface (Zhou, Ralston, Sedev, & Beattie, 2009). However, in a medium of high ionic strength, the charges on the surface of the nanoparticles are screened and aggregation occurs (Pamiés et al., 2014; Zhao, Li, & Xie, 2015). In a previous work (Collado-González et al., 2015) we studied the aggregation process of gold-citrate nanoparticles in the presence of chitosan. Our hypothesis for this work is that chitosan is suitable for stabilizing not only small metallic gold-citrate nanoparticles but also the larger silk fibroin nanoparticles, forming nanocomposites that could be used as nanocarriers for controlled drug delivery and that the characteristics of the final nanocomposites will depend significantly on the proportion of chitosan used to obtain the nanoparticles.

Because of their physical, chemical and biological properties, silk fibroin nanoparticles (SFN) (see, for example, Mottaghitalab, Farokhi, Shokrgozar, Atyabi, & Hosseinkhani, 2015) and citrate-gold nanoparticles (AuNP) (see, for example, Hu, Du, Li, Fan, & Li, 2015) are biodegradable and biocompatible materials, which can be processed into a range of structural forms. Stable suspensions in water of SFN can be achieved using different methodologies (Lozano-Pérez et al., 2015). Stable AuNP are usually obtained through reduction in a medium with citrate (Corzo Lucioni, 2012). In order to prevent aggregation, efforts have been made to synthesize chitosan-gold nanocomposites using either gold precursors (Jin et al., 2013) or gold nanoparticles (Prado-Gotor, López-Pérez, Martín, Cabrera-Escribano, & Franconetti, 2014; Collado-González

* Corresponding author.
E-mail address: fgb@um.es (F.G. Díaz Baños).

http://dx.doi.org/10.1016/j.carbpol.2016.12.043
0144-8617/

et al., 2015). In addition, some groups have studied structures composed of silk fibroin, which tend to self-assemble in different conditions (Vepari & Kaplan, 2007), and chitosan (Bhardwaj & Kundu, 2011) or chitosan derivatives (Wang et al., 2015). However, the literature contains no specific studies on the stabilizing role of chitosan on SFN.

The electrostatic interactions that occur between chitosan and citrate-gold nanoparticles have received attention previously (Huang & Yang, 2003). Regarding chitosan-SFN nanocomposites, in this paper we include some computational modelling and calculations to try to understand at the atomic level which atoms are involved in the interactions. With the structural information that is available for the molecules of interest, computer simulation methods can provide useful predictions concerning the process of interest and can also aid in the interpretation and analysis of experimental data (MacKerell et al., 1998). Of the different potential molecular modeling methods available for the study of encapsulation, we used blind docking calculations, which consist of the computer simulation of the energies involved in the protein-ligand interactions (Sánchez-Linares, Pérez-Sánchez, Cecilia, & García, 2012). Among the results obtained by such simulations is informative on how many different chitosan molecules interact with SFN, which protein residues are involved, how these interactions are established (electrostatic, van der Waals, hydrogen bonds, hydrophobic, etc), and what the main protein-ligand interactions are (Navarro-Fernández et al., 2012).

2. Materials and methods

2.1. Chitosan

Chitosan was obtained from Sigma-Aldrich (448877-250G). The molecular weight was in the order of 250,000 Da and the degree of acetylation around 20% (data from the manufacturer). Chitosan solutions at $c = 10^{-3}\,g\,cm^{-3}$ were prepared at pH 3.5–4 (glacial acetic acid from Panreac was used to adjust pH) stirring overnight. These solutions were later diluted (with water at pH ≈ 3.5–4) to obtain final concentrations equal to $10^{-4}\,g\,cm^{-3}$, $10^{-5}\,g\,cm^{-3}$, $10^{-6}\,g\,cm^{-3}$ and $10^{-7}\,g\,cm^{-3}$. In order to study the polymer's behavior in solution as a function of concentration, two different preparations of chitosan at pH 3.5–3.6 and concentrations of $c = 10^{-3}\,g\,cm^{-3}$, $c = 10^{-5}\,g\,cm^{-3}$, and $c = 10^{-7}\,g\,cm^{-3}$ were analyzed.

The following method can be used to roughly calculate the number of chitosan molecules present in the different samples. Assuming a molecular weight of 250,000 g/mol, on average, each molecule will weigh 4.2×10^{-19} g. When $c = 0.001\,g/cm^3$, these will be 2.4×10^{15} molecules of chitosan in each cm^3.

2.2. Gold nanoparticles

Gold nanoparticles coated by a negatively charged citrate layer were obtained from Ted Pella, Inc. (Redding, CA) in the form of a suspension in water with a content of 5.7×10^{12} particles/cm^3. We confirmed that the hydrodynamic diameter was 13 nm (nominal value 10 nm).

2.3. Silk fibroin nanoparticles

To obtain SFNs, silk fibroin was dissolved in ionic liquids and submitted to high-power ultrasounds as described previously (Lozano-Pérez et al., 2015). A suspension was prepared with freeze-dried SFN at a final concentration of to $10^{-4}\,g/cm^3$, and subjected to pulsating ultrasonication of 15" steps at 30% amplitude for a total time of 3 min in a Sonifier Branson 450D (Emmerson Ultrasonic Corporation. Dansbury, USA). These colloidal suspensions of SFNs remained stable in water for approximately 3 months before aggregation occurred.

2.4. Chitosan-gold nanocomposites

These nanocomposites were prepared mixing chitosan and citrate gold nanoparticles at different proportions at pH = 4. To facilitate the analysis of the results, the composition of each sample is expressed as particles of gold per molecules of chitosan in the sample. As 0.5 cm^3 of AuNP suspension was added in all preparations, the final content of AuNP was 2.85×10^{12} nanoparticles per sample. Prado-Grotor et al. (Prado-Gotor, López-Pérez, Martín, Cabrera-Escribano, & Franconetti, 2014) calculated that the mean number of Au atoms in a spherical gold nanoparticle of 10 nm is 30687. Thus, taking into account the atomic weight of gold, every sample contained 2.88×10^{-5} g of gold. Then, a mixture of 0.5 cm^3 of AuNP and 1 cm^3 of CS 0.001 g/cm^3 can be roughly described as a proportion of 3×10^{-2}:1 (in weight) or $1{:}10^3$ (in number of particles) of AuNP:CS. We chose the second option and, with this, AuNP:CS samples of $1{:}10^3$, $1{:}10^2$, 1:10 and 1:1 were prepared.

2.5. Chitosan-silk fibroin nanocomposites

These nanocomposites were prepared mixing chitosan and silk fibroin nanoparticles at different proportions at pH = 4 (for details see Table 1 SM, where SM means supplementary material). The amount of SFN in the sample was fixed at 10^{-4} g and the prepared proportions were CS:SFN 1:0.4, 1:0.8, 1:1.6, 1:3.2, 1:6.35, 1:12.7, 1:25.4, 1:50.8, 1:203, and 1:813 mg:mg (in weight).

2.6. Ionic strength

To evaluate the effect of the ionic strength of the medium, different concentrations of KNO_3 (from Probus, S.A.) were used. MilliQ water was used in all the preparations.

2.7. Size and z potential measurements

Hydrodynamic size was measured by Dynamic Light Scattering using a Malvern Zetasizer Nano ZS (Malvern Instruments Ltd, UK) at 25 °C and a 173° angle relative to the source. The incorporated software calculates the hydrodynamic diameter distribution from the time autocorrelation function of the scattering intensity fluctuations. For chitosan solutions, to improve reproducibility, each assay was composed of 300 measurements (5 runs of 20 s each with no delay between measurements). For CS-AuNP and CS-SFN each assay was composed of 3 measurements (10 runs of 10 s) and took 5–8 min, what means that t = 0 is equivalent to this time. Later, two more results were obtained at $t \approx 1.5$ and $t \approx 24$ h. Each curve in a plot represents the average of all performed measurements. For nanocomposites, a first control measurement was made to a suspension of nanoparticles (AuNP or SFN) followed by a second measurement when chitosan solution was added that was as time 0 in salt-free suspensions. In samples in which the ionic strength was increased, a third measurement was carried out when KNO_3 was added, taking the third measurement as time 0. This protocol was confirmed as giving very reproducible results.

In this work, we have included results for the distributions by intensity and by number. The Malvern software (included in the apparatus) provided the size distribution by number from the primary distribution by intensity assuming, in addition to the sphericity and homogeneity of particles and the accuracy of the distribution by intensity, the precise knowledge of the actual refractive index of the particles (we checked that the influence of this factor was very small for our system). Thus, the distribution by intensity must be considered in order to characterize particle size,

whereas distribution by number is suitable for estimating relative populations of the particles when comparing results from different conditions.

The zeta potential, ζ, was also measured with the same apparatus. Each assay consisted of 6 measurements taken in an automated way.

2.8. Blind docking calculations

For the blind docking calculations, a representative protein X-ray crystal structure for silk fibroin was chosen from the Protein Data Bank (PDB) database with PDB identifier 3UA0 (He et al., 2012). The full-atom model of the protein used in this study was prepared from the raw PDB structure 3UA0 by removing water molecules, adding hydrogen atoms, assigning the ionization states of the amino acids using the Protonate3D function of the MOE software package and by calculating atomic partial charges using the AMBER99 forcefield (Wang et al., 2015) implemented in MOE.

For chitosan, the model consisting of a carbohydrate nonamer previously developed by Cunha et al. (2012) was used.

The docking of chitosan to the prepared protein structure model of silk fibroin and the detailed binding energy calculations were performed with the Autodock Vina docking software (Trott & Olson, 2010) using default configuration parameters. The size of the grid box for ligand docking was set to extend 120 Å in each direction from the geometric center of each individual docking simulation. The docking score produced by Autodock Vina was taken as the predicted value of the ligand binding energy. Only the top-ranked poses were used for structural and energy analyses. The scoring function from Vina considers the Lennard-Jones term (LJ), hydrogen bonds (H-bonds), electrostatic interactions, hydrophobic stabilization, entropic penalty due to the number of rotatable bonds, and the internal energy of the ligand. A blind docking approach was followed (Navarro-Fernández et al., 2012) in which, multiple docking runs started around geometric centres of all the residues within the selected threshold. A histogram with the resulting distribution of binding energies and their structural clusters of poses is generated.

3. Results and discussion

3.1. Chitosan behavior

The behavior of chitosan in solution was studied in a previous work of our group (Collado-González et al., 2015), where it was seen that the distribution of sizes of chitosan and its structures at a final concentration of 10^{-3} g cm^{-3} and at pH = 4 spanned from 80 nm to 8000 nm. In this work the pH were fixed at pH = 3.5-3.6 with similar results. The chitosan concentration used was about the critical overlap concentration, c* = 0.0008 g/cm^3, for our CS solution (Cho et al., 2013; Morariu, Brunchi, & Bercea, 2012) and can be considered as a non-dilute solution. Thus, the CS chains form aggregates of various sizes, whose characteristics will depend on both the CS intrinsic features (i.e. chain length) and the environmental conditions (Korchagina & Philippova, 2010; Popa-Nita, Alcouffe, Rochas, David, & Domard, 2010; Schatz et al., 2003). Since dilution of the chitosan solutions was expected to decrease the tendency to entangle, we used final concentrations equal to 10^{-5} g cm^{-3} and 10^{-7} g cm^{-3}. As can be seen in Fig. 1, when solutions are diluted to values of 10^{-5} g cm^{-3} or lower, aggregates larger than 1000 nm do not appear. In fact, when the chitosan concentration decreased, the size of the aggregates was also found to decrease. Indeed, most molecules of chitosan were found on their own or in very small aggregates (diameter lower than 100 nm) and only a small portion were observed forming entanglements of a few hundreds of nanometers.

In order to study the behavior of chitosan in a medium with a high ionic force, the ionic strength was set at 0.15 M and 0.25 M. As we observed in a previous work using a different concentration (Collado-González et al., 2015), the presence of salt (I = 0.15 M and 0.25 M gave the same results) decreases the hydrodynamic size of chitosan molecules and also decreases their tendency to form aggregates (see Figs. 1 and 2S M). From the data in the literature (Morris, Castile, Smith, Adams, & Harding, 2009) we calculated (Collado-González et al., 2015) the expected hydrodynamic diameter of our free chitosan chains in solution with similar features and dissolved in similar saline conditions as ours, obtaining a range of 50–80 nm. Therefore, the peak shown in Fig. 2 at 80 nm in diluted conditions (10^{-7} g/cm^3) was most probably due to free chitosan chains. Additionally, the disentanglement of chitosan aggregates can be clearly appreciated in the distribution by number. In this plot, it can be seen that in conditions of high ionic strength aggregates greater than 100 nm are considerably reduced in number.

Our results fit well with the idea that in non-diluted conditions (10^{-3} g cm^{-3}), the probability of entanglement among polymer chains increases because of the number of molecules and their expanded conformation. At low concentrations, the number of chitosan molecules interacting decreases, and when the ionic force of the solution increases, repulsive forces between the positive internal charges on the chains decrease and the hydrodynamic size of the particles is reduced. In this case there is an increase in free chitosan chains. Taken together these results can be considered relevant for the preparation of nanocomposites based on chitosan.

3.2. Chitosan and citrate-gold nanoparticles

Citrate-gold nanoparticles (AuNP) tend to aggregate when the ionic strength of the medium increases (Fig. 3SM). However, in previous a work (Collado-González et al., 2015), it was seen that AuNP and chitosan interact to form nanocomposites are formed, demonstrating the role of chitosan in preventing nanoparticle aggregation in conditions of high ionic strength. In the present study, we wanted to find the best proportion AuNP:CS ratio to prevent AuNP aggregation and provide the smallest nanocomposites.

The nanocomposites obtained varied widely in size depending on the AuNP:CS ratio and salt conditions (Figs. 3 and 4, also 4SM). A careful look at these results shows two extreme situations. For a AuNP:CS proportion 1:10^3 (with CS concentration in the order of 10^{-3} g cm^{-3}), three stable populations of nanocomposites could be distinguished in the intensity plot. Before the addition of salt, the largest sizes (300 nm and more, even microstructures) were above the desirable value. Some of the nanoparticles obtained had a size in the order of 50 nm. Although it might be seen surprising, the number plot indicated that for both populations, the number of particles was low compared with the small structures in the order of 20 nm. The situation changed drastically when salt was added and only two populations were detected. The bigger one is shown by a peak that becomes narrower around 200 nm and the second centered of about 20 nm. This behavior resembles that observed previously in similar conditions (Collado-González et al., 2015), and is compatible with the idea that, at this concentration, some of the chitosan molecules, probably the longest ones, tend to be entangled and the presence of salt and AuNP decreases the hydrodynamic size of the aggregates and individual molecules of chitosan and nanocomposites.

At the other extreme we may look the sample with the lowest proportion of chitosan (AuNP:CS 1:1, CS concentration comparable to 10^{-7}). When no salt is added, very few big nanocomposites are obtained (see intensity plot, Fig. 3) and a quasi single broad peak around 30 nm is observed. Most (in number) nanoparticles formed have the same size as the smallest of AuNP:CS 1:10^3. But in this case, the nanocomposites obtained are not stable and a strong and very

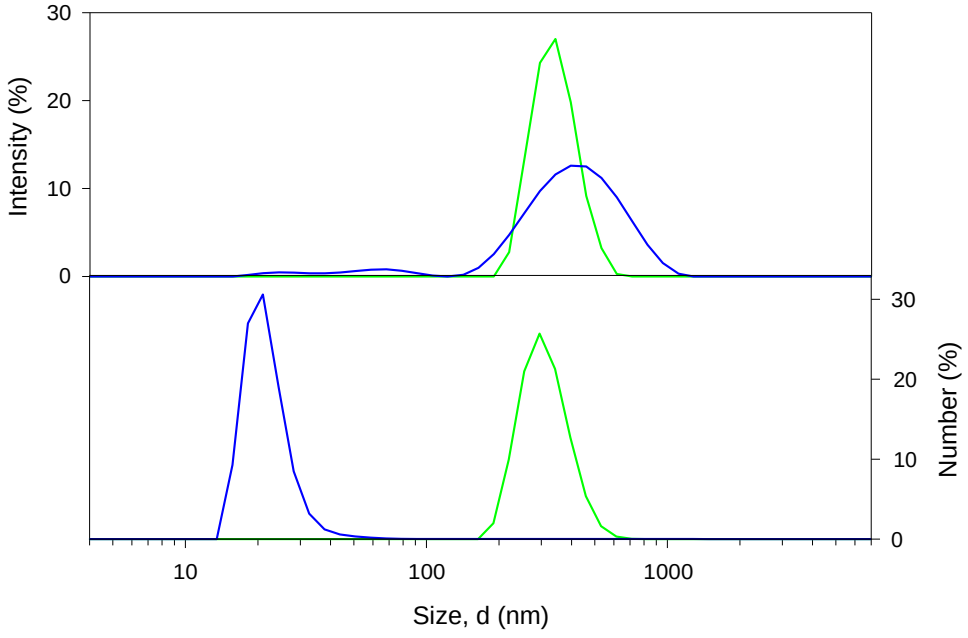

Fig. 1. Size of the particles present in chitosan solutions at different concentrations with ionic force equal to 0 M: 10^{-3} g/cm^3 (red line), 10^{-5} g/cm^3 (green line), 10^{-7} g/cm^3 (blue line). (For interpretation of the references to colour in this figure legend, the reader is referred to the web version of this article.)

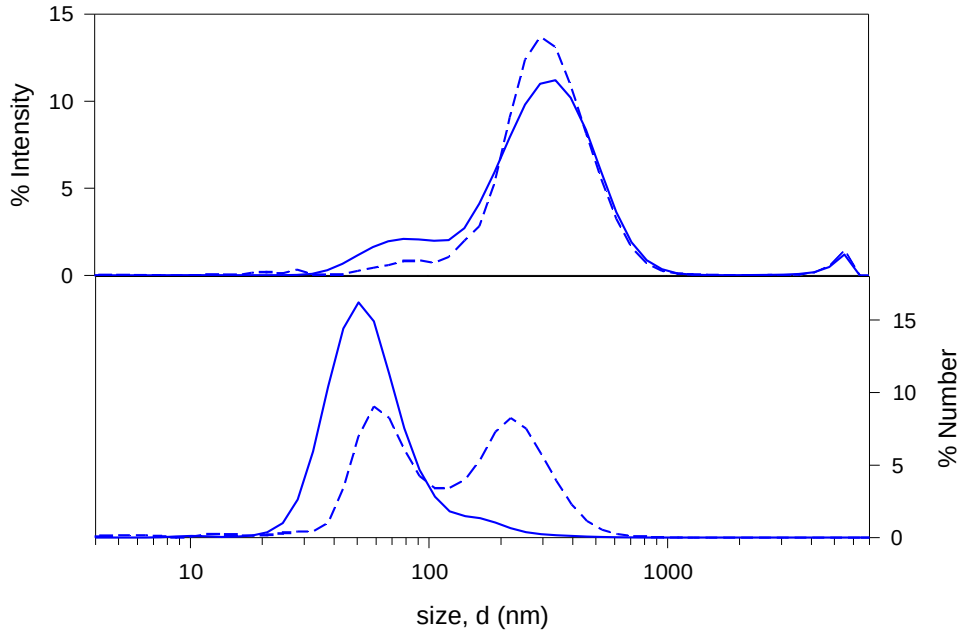

Fig. 2. Sizes of the particles present in solutions of chitosan at 10^{-7} g/cm^3 at different ionic forces 0 M (dashed line) or 0.15 M (solid line).

fast aggregation and sedimentation occurs (Fig. 4, also Fig. 4SM). Thus, the hypothesis concerning the lack of polymer to prevent the AuNP nanoparticle aggregation was reinforced.

Samples containing amounts of chitosan between those mentioned in the above paragraphs showed an intermediate behavior. Sample with a proportion of 1:10^2 formed two populations of nanocomposites that became a single one with most structures below 100 nm, although an asymmetric peak in the intensity plot showed that a few bigger structures are also present. The most interesting are the nanocomposites of the sample AuNP:CS 1:10, which showed a single and relatively narrow distribution in all conditions. Size of these nanocomposites changed from 230 nm in salt-free suspension to 130 nm when salt was added.

Z potential allows us to know the structure of the nanocomposites in terms of the distribution and balance of superficial charges. For nanocomposites composed of AuNP and chitosan, values change from +32 mV for AuNP:CS 1:10^2 to -25 mV for AuNP:CS 1:10 (see Table 2SM). The reason of these values must the amount of AuNPs bound on the surface of chitosan, aggregates becoming more negative when the proportion of AuNP increased.

In brief, we already knew that chitosan (in moderate concentrations) interacts with gold nanoparticles to give nanocomposites (with a positive Z potential) that remain stable when the ionic

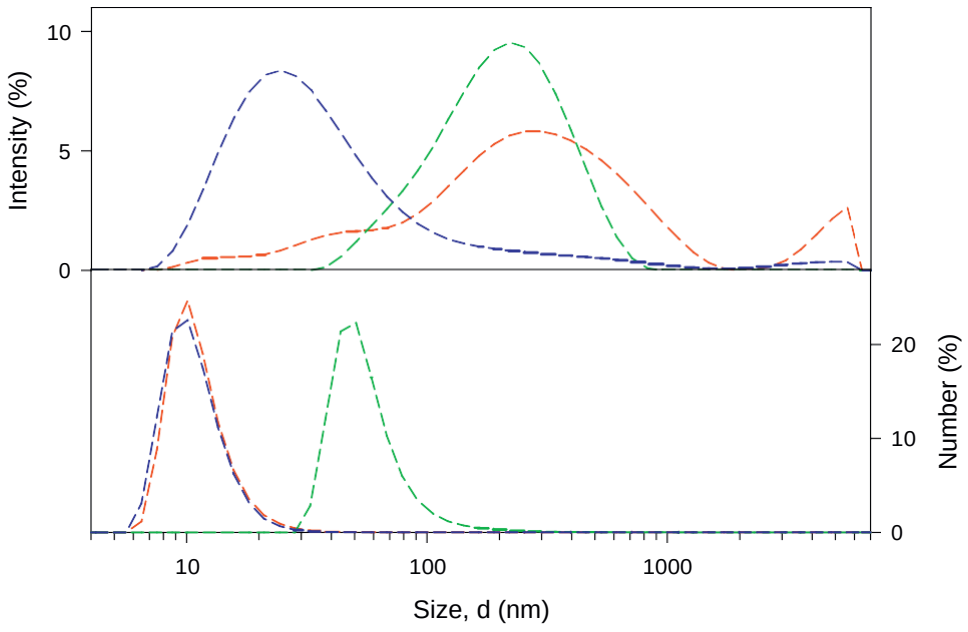

Fig. 3. Sizes of the nanocomposites, when no salt was added to the medium, obtained from different ratios AuNP:CS: $1{:}10^3$ (red), 1:10 (green), 1:1 (blue). (For interpretation of the references to colour in this figure legend, the reader is referred to the web version of this article.)

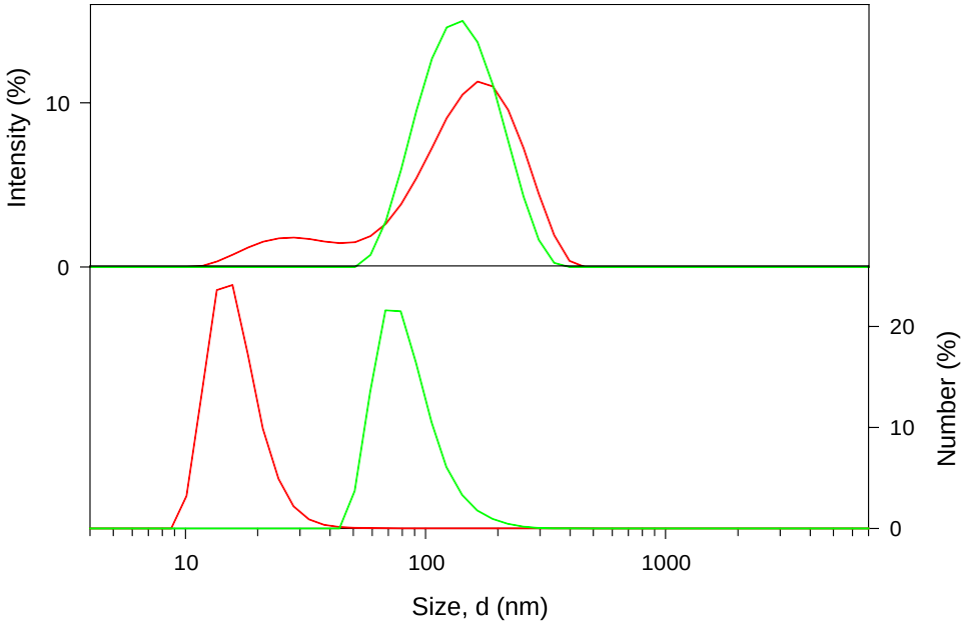

Fig. 4. Sizes of the nanocomposites exposed to 0.15 M for 24 h. The ratios AuNP:CS are: $1{:}10^3$ (red line) and 1:10 (green line). AuNP:CS 1:1 signal was not observable. (For interpretation of the references to colour in this figure legend, the reader is referred to the web version of this article.)

strength is increased (Collado-González et al., 2015). Now we have shown that a proportion gold nanoparticles:chitosan 1:10 yielded well defined (in size) nanocomposites with negative Z potential which are stable at high ionic strength. We must point out that the responsible of this colloidal stability cannot be only the electrostatic repulsion. We have already shown for AuNP that, at this ionic strength, charges are screened and aggregation is produced (Pamiés et al., 2014). On the other hand, at this ionic strength, chitosan remained soluble and no big aggregates were formed. Then, it is plausible to think in the supporting chitosan skeleton as the responsible of the lyophilic character of the AuNP:CS nanocomposites.

3.3. *Chitosan-silk fibroin nanocomposites*

We studied nanocomposites formed by mixing different proportions of chitosan and silk fibroin in water (see Table 1SM). We found a range of ratios CS:SFN (roughly between 1:50.8 and 1:1.6) in which nearly all particle initially present are forming nanocomposites with a size around 200 nm (Fig. 5 and 5SM) which is just

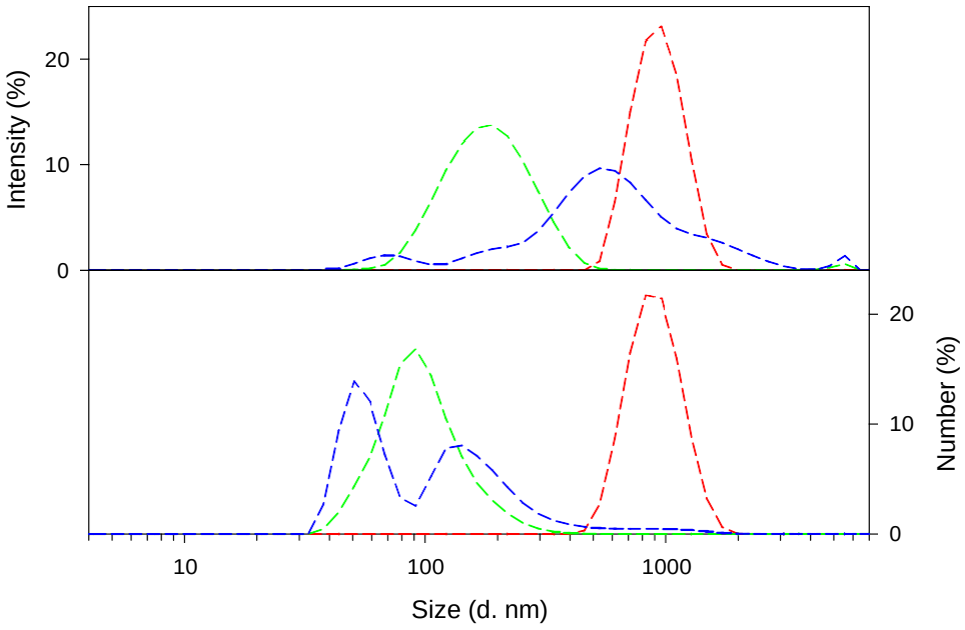

Fig. 5. Size of the nanocomposites CS-SFN when the ionic strength of the medium was not increased. The different proportions represented are CS:SFN 1:203 mg:mg (red line), CS:SFN 1:12.7 mg:mg (green line) and CS:SFN 1:0.4 mg:mg (blue line). Fig. 4SM includes all the cases studied. (For interpretation of the references to colour in this figure legend, the reader is referred to the web version of this article.)

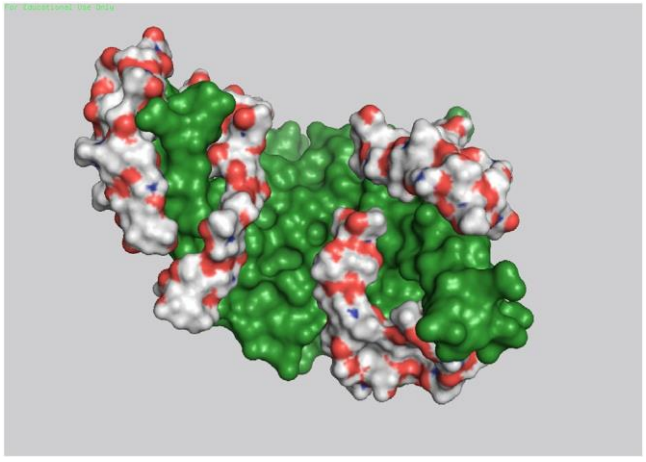

Fig. 6. Surface representation of detected interaction areas between SFN (green) and chitosan (using white for carbon skeleton) by the blind docking method. (For interpretation of the references to colour in this figure legend, the reader is referred to the web version of this article.)

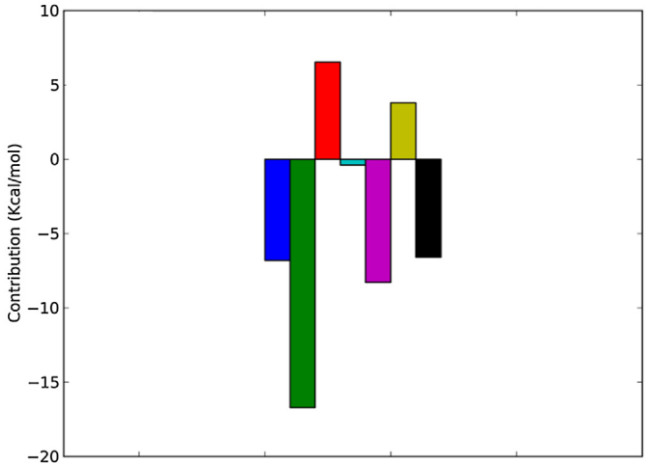

Fig. 7. Energetic analysis of the top chitosan pose docked to the SFN monomer model. Representation of the values of the different energetic contributions to the predicted binding energy (Kcal/mol) where depicted energetic contributions are; electrostatic interaction types Gauss1 and Gauss2 (blue and green), repulsion forces (red), hydrophobic interactions (light blue), hydrogen bonds (pink), entropic contribution (yellow) and total predicted binding energy (black). (For interpretation of the references to colour in this figure legend, the reader is referred to the web version of this article.)

slightly larger than the size of SFNs. All these nanocomposites were stable in water at least 24 hours (Fig. 6SM).

Results obtained from blind docking calculations provide details on how chitosan interacts with SFN by means of different types of intermolecular interactions. In Fig. 7SM it can be seen that a maximum of 5 "molecules" of chitosan (remember that our model is a nonamer) can bind to SFN, and that there is a maximum difference of 4 units in the scoring function values between the top and lowest poses. This suggests that there are certain preferred areas for the docking of chitosan in the SFN monomer model. Moreover, a good steric fit between the five predicted clusters of poses and the protein is obtained, as shown in Fig. 6. This steric fit is mainly due to electrostatic interactions, as shown by blue and green bars in Figs. 7 and 8.

If we take into account the size of the nanocomposites, the values of the Z potential (Table 4SM) and blind docking calculations, we find that the most feasible explanation is that the SFN are inside of the structures formed and the chitosan is surrounding the nanoparticles interacting with the negatively charged areas of the SFN. This idea fits very well with a structure like that showed by Wang et al. (2015). In addition, it seems that for higher proportions of SFN, the CS molecules could act as bridges between SFN particles forming structures in the range of microns (Fig. 5). Moreover, when chitosan proportion is very low (CS:SFN 1:813 mg:mg), nanocomposites still have negative Z potential or low positive Z potential (CS:SFN 1:203 mg:mg). It seems that due to the small amount of CS in the sample, this polymer cannot completely coat the SFN and, as a consequence, the electrostatic repulsion forces are not sufficiently strong to prevent the formation of large aggregates even in water. On the other hand, when the amount of SFN in the mixture

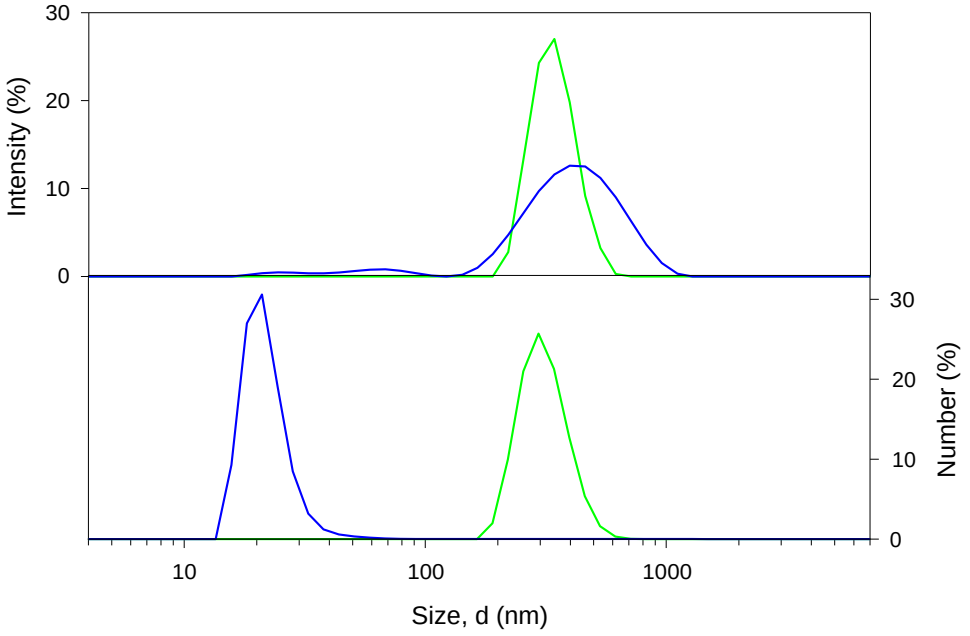

Fig. 8. Size of the nanocomposites obtained from chitosan and silk fibroin nanoparticles in different proportions exposed to an ionic strength 0.024 M for 24 h. The proportions areCS:SFN 1:12.7 mg:mg (green) and CS:SFN 1:0.4 mg:mg (blue). The CS:SFN 1:203 mg:mg signal was not observable. (For interpretation of the references to colour in this figure legend, the reader is referred to the web version of this article.)

was lower than a ratio 1:0.4 (Fig. 5SM), the characteristics of the sample were similar to those of a chitosan solution. Between them, we found (Fig. 5) the distribution for the CS:SFN ratio 1:12.7, with a maximum around 190 nm.

In addition to electrostatic interactions between chitosan and the protein, the stabilizing binding interaction is due to a network of hydrogen bonds (pink bar in Fig. 7). The fact that the SFN monomer can interact with a certain number (5 in our model) of chitosan molecules implies that variations in the concentration of chitosan could affect the stabilization process of SFN, as observed experimentally in this work.

Silk fibroin nanoparticles are not stable when ionic strength of the dispersion is increased. In this work, we performed experiments to assess the stabilizing effect of the chitosan on the SFN when salt is added to the medium. A previous paper studied the stabilizing effect of glycol chitosan (Wang et al., 2015), soluble at neutral pH, in nanocomposites very similar to ours. We used a different and complementary approach and we estimated the minimum ionic strength at which SFN showed a slow but strong aggregation. In order to study the effect of different ratios CS:SFN to prevent aggregation, we chose I = 0.024 M (Table 3SM and Fig. 8SM). We checked that higher values induced very fast aggregation.

After mixing chitosan and silk fibroin nanoparticles (Fig. 9S M) it was seen that, when the amount of chitosan in the sample was equal to or lower than the proportion CS:SFN 1:50.8 mg:mg, aggregation was observed even at short times. But, for ratios in the range 1:25.4 to 1:1.6 the structures had a size in the order of 200–300 nm a few minutes after mixing.

After 24 h since the addition of the salt, the sample which contains chitosan and SFN in a proportion of 1:25.4 mg:mg formed microcomposites. The amount of chitosan was not sufficient to prevent the slow aggregation of the SFN at this ionic strength. But samples containing proportions CS:SFN ranging from 1:12.7 mg:mg to 1:1.6 mg:mg did not aggregate, yielded populations of a few hundred nanometers (Fig. 10S M). Besides, the standard deviation of these populations was small. The most interesting cases were CS:SFN 1:6.35 mg:mg with a peak in the intensity distribution at 315 ± 34 nm of hydrodynamic diameter and CS:SFN 1:12.7 mg:mg with a peak at 344 ± 72 nm. In both cases the homogeneity of these nanocomposites was bigger than the rest of the samples. These nanocomposites aggregated very fast when ionic strength was 0.15 M.

At CS:SFN proportions of 1:0.4 mg:mg and lower, a peak in the range of few nanometers was observed. A plausible explanation could be that when chitosan is in excess, longer chains of chitosan interact with silk, while some of the shorter chains remain free.

In a previous work (Wang et al., 2015) glycol chitosan (GCS) was used to stabilize silk fibroin nanoparticles in water and physiological liquids. Although the concentrations and proportions GCS:SFN were similar to those used in this work, their nanocomposites did not aggregate in high ionic strength conditions. We have shown that the main interaction between chitosan and fibroin was electrostatic and that CS:SFN nanocomposites were stable at I = 0.024 M but not at physiological ionic strength. It must be concluded therefore that the glycol group was responsible for preventing the aggregation of the nanocomposites. A plausible explanation is that this group was able to transform a lyophobic colloid into a lyophilic colloid. The stability of lyophilic colloids is not be significantly affected by the screening effect of the ions in a medium with high ionic strength.

4. Conclusion

The role of chitosan as stabilizing agent for negatively charged nanoparticles is clear, since this polymer prevents the aggregation which takes place when the ionic strength of the medium is increased. In this work we have shown that the proportion of the two components (chitosan and AuNP or SFN) and the concentration of chitosan have a significant influence on the nanocomposites obtained. In both cases an optimum value is proposed to obtain the smallest and most homogeneous stable nanocomposites.

Our results show two different ways in which this might occurs: (i) chitosan acts as a structure on whose surface negatively charged small gold nanoparticles are immobilized, and (ii) the chitosan molecules surround the silk fibroin nanoparticles mainly through electrostactic interactions at well defined sites. In this case, the

stabilizing effect of chitosan is limited by the screening effect of salt ions, which decrease the effect of repulsive electrostatic forces. The use of chitosan derivatives could overcome this constraint, transforming the lyophobic character of the colloidal particle into lyophilic.

Acknowledgements

This work was partially supported by the European Commission (FEDER/ERDF) and the Spanish MINECO (Ref. CTQ2011-25613 and Ref. CTQ2014-57467-R), the Seneca Foundation of Science and Technology of Murcia (Projects 19499/PI/14 and 18946/JLI/13), the supercomputing infrastructure of the NLHPC (ECM-02) and the computing facilities of Extremadura Research Centre for Advanced Technologies (CETA CIEMAT). The authors also thankfully acknowledge the computer resources and the technical support provided by the Plataforma Andaluza de Bioinformática of the University of Málaga. Mercedes G. Montalbán acknowledges support from Spanish MINECO (FPI grant, BES-2012-053267).

Appendix A. Supplementary data

Supplementary data associated with this article can be found, in the online version, at http://dx.doi.org/10.1016/j.carbpol.2016.12.043.

References

Bhardwaj, N., & Kundu, S. (2011). Silk fibroin protein and chitosan polyelectrolyte complex porous scaffolds for tissue engineering applications. *Carbohydrate Polymers, 85,* 325–333.

Cho, J., Bégin, A., & Carreau, P. (2006). Viscoelastic properties of chitosan solutions: Effect of concentration and ionic strength. *Journal of Food Engineering, 74,* 500–515.

Cho, E., Holback, H., Liu, K., Abouelmagd, S., Park, J., & Yeo, Y. (2013). Nanoparticle characterization: State of the art, challenges, and emerging technologies. *Molecular Pharmaceutics, 10,* 2093–2110.

Collado-González, M., Fernández Espín, V., Montalbán, M., Pamiés, R., Hernández Cifre, J., Díaz Baños, F. G., Villora, G., & García de la Torre, J. (2015). Aggregation behaviour of gold nanoparticles in presence of chitosan. *Journal of Nanoparticles Research, 17,* 268.

Corzo Lucioni, A. (2012). Síntesis de nanopartículas do oro obtenidas por reducción de H[AuCl4]? *Revista de la Sociedad Química del Perú, 78*(2), 79–90.

Cunha, R., Franca, E., Pontes, F., Lius, R., Soares, T., & Rusu, V. (2012). *The molecular structure and conformational dynamics of chitosan polymers: an integrated perspective from experiments and computational simulations.* INTECH Open Access Publisher.

Delmar, K., & Bianco-Peled, H. (2015). The dramatic effect of small pH changes on the properties of chitosan hydrogels crosslinked with genipin. *Carbohydrate Polymers, 127,* 28–37.

Domard, A. (2011). A perspective on 30 years research on chitin and chitosan. *Carbohydrates Polymers, 84,* 696–703.

He, Y.X., Zhang, N.N., Li, W.F., Jia, N., Chen, B.Y., Zhou, K., Zhang, J., Chen, Y., & Zhou, C.Z. (2012). N-Terminal Domain of Bombyx mori Fibroin Mediates the Assembly of Silk in Response to pH Decrease. J.Mol.Biol. 418: 197-207. Data obtained from Protein Data Bank (http://www.rcsb.org/pdb). PDB ID: 3UA0. Last accessed 06/09/2016.

Hu, Y., Du, C., Li, Y., Fan, L., & Li, X. (2015). A gold nanoparticle-based colorimetric probe for rapid detection of 1-hydroxypyrene in urine. *Analyst, 140,* 4662–4667.

Huang, H., & Yang, H. (2003). Chitosan mediated assembly of gold nanoparticles multilayer. *Colloids and Surfaces A: Physicochemical Engineering Aspects, 226,* 77–86.

Jin, Y., Li, Z., Hu, L., Shi, X., Guan, W., & Du, Y. (2013). Synthesis of chitosan-stabilized gold nanoparticles by atmospheric plasma. *Carbohydrate Polymers, 91,* 152–156.

Korchagina, E., & Philippova, O. (2010). Multichain aggregates in dilute solution of associating polyelectrolyte keeping a constant size at the increase in the chain length of individual macromolecules. *Biomacromolecules, 11,* 3457–3466.

Leiva, A., Bonardd, S., Pino, M., Saldías, C., Kortaberria, G., & Radic, D. (2015). Improving the performance of chitosan in the synthesis and stabilization of gold nanoparticles. *European Polymer Journal, 68,* 419–431.

Lozano-Pérez, A., García Montalbán, M., Aznar-Cervantes, S., Cragnolini, F., Cenis, J., & Víllora, G. (2015). Production of silk fibroin nanoparticles using ionic liquids and high-power ultrasound. *Journal of Applied Polymer Science, 132,* 41702.

Luo, Y., Teng, Z., Li, Y., & Wang, Q. (2015). Solid lipid nanoparticles for oral drug delivery: Chitosan coating improves stability, controlled delivery, mucoadhesion and cellular uptake. *Carbohydrate Polymers, 122,* 221–229.

MacKerell, A. D., Bashford, D., Bellott, M., Dunbrack, R. L., Evanseck, J. D., Field, M. J., et al. (1998). All-atom empirical potential for molecular modeling and dynamics studies of proteins. *Journal of Physical Chemistry B, 102,* 3586–3616.

Morariu, S., Brunchi, C., & Bercea, M. (2012). The behaviour of chitosan in solvents with different ionic strength. *Industrial and Engineering Chemistry Research, 51,* 12959–12966.

Morris, G., Castile, J., Smith, A., Adams, G., & Harding, S. (2009). Macromolecular conformation of chitosan in dilute solution: A new global hydrodynamic approach. *Carbohydrate Polymers, 76,* 616–621.

Mottaghitalab, F., Farokhi, M., Shokrgozar, M., Atyabi, F., & Hosseinkhani, H. (2015). Silk fibroin nanoparticle as a novel drug delivery system. *Journal of Controlled Release, 206,* 161–176.

Navarro-Fernández, J., Pérez-Sánchez, H., Martínez-Martínez, I., Meliciani, I., Guerrero, J., Vicente, V., Corral, J., & Wenzel, W. (2012). In silico discovery of a compound with nanomolar affinity to antithrombin causing partial activation and increased heparin affinity. *Journal of Medicinal Chemistry, 55,* 6403–6412.

Pamiés, R., Hernández Cifre, J., Fernández Espín, V., Collado-González, M., Díaz Baños, F., & García de la Torre, J. (2014). Aggregation behaviour of gold nanoparticles in saline aqueous media. *Journal of Nanoparticle Research, 16,* 2376.

Popa-Nita, S., Alcouffe, P., Rochas, C., David, L., & Domard, A. (2010). Continuum of structural organization from chitosan solutions to derived physical forms. *Biomacromolecules, 11,* 6–12.

Prado-Gotor, R., López-Pérez, G., Martín, M., Cabrera-Escribano, F., & Franconetti, A. (2014). Use of gold nanoparticles as crosslink agent to form chitosan nanocapsules: Study of the direct interaction in aqueous solutions. *Journal of Inorganic Biochemistry, 135,* 77–85.

Raferty, R., Tierney, E., Curtin, C., Cryan, S., & O'Brien, F. (2015). Development of a gene-activated scaffold plarform for tissue engineering applications using chitosan-pDNA nanoparticles on collagen-based scaffolds. *Journal of Controlled Release, 210,* 84–94.

Sánchez-Linares, I., Pérez-Sánchez, H., Cecilia, J., & García, J. (2012). High-throughtput parallel blind virtual screeing using BINDSURF. *BMC Bioinformatics, 13*(Suppl. 14), S13.

Schatz, C., Viton, C., Delair, T., Pichot, C., & Domard, A. (2003). Typical physicochemical behaviours of chitosan in aqueous solution. *Biomacromolecules, 4,* 641–648.

Trott, O., & Olson, A. (2010). AutoDock Vina: Improving the speed and accuracy of docking with a new scoring function, efficient optimization, and multithreading. *Journal of Computational Chemistry, 31,* 455–461.

Vepari, C., & Kaplan, D. (2007). Silk as a biomaterial. *Progress in Polymer Science, 32,* 991–1007.

Wang, S., Xu, T., Yang, Y., & Shao, Z. (2015). Colloidal stability of silk fibroin nanoparticles coated with cationic polymer for effective drug delivery. *ACS Applied Materials and Interfaces,*

Zakaria, H., Shah, A., Konieczny, M., Hoffmann, J., Nijdam, A., & Reeves, M. (2013). Small molecule- and amino acid-induced aggregation of gold nanoparticles. *Langmuir, 29,* 7661–7673.

Zhao, Z., Li, Y., & Xie, M. (2015). Silk fibroin-based nanoparticles for drug delivery. *International Journal of Molecular Sciences, 16,* 4880–4903.

Zhou, J., Ralston, J., Sedev, R., & Beattie, D. (2009). Functionalized gold nanoparticles: Synthesis, structure and colloid stability. *Journal of Colloid and Interface Science, 331,* 251–262.